EXPERIMENTAL STUDY OF FLOW AND HEAT TRANSFER IN A ROTATING CHEMICAL VAPOR DEPOSITION REACTOR

BY SUN WONG

A thesis submitted to the

Graduate School—New Brunswick

Rutgers, The State University of New Jersey

in partial fulfillment of the requirements

for the degree of

Master of Science

Graduate Program in Mechanical and Aerospace Engineering

Written under the direction of

Professor Yogesh Jaluria

and approved by

_____

_____

_____

_____

New Brunswick, New Jersey

May, 2015

ABSTRACT OF THE THESIS

Experimental Study of Flow and Heat Transfer in a Rotating Chemical Vapor Deposition Reactor

by Sun Wong

Thesis Director: Professor Yogesh Jaluria

An experimental model was set up to study the rotating vertical impinging chemical vapor deposition reactor. Deposition occurs only when the system has enough thermal energy. Therefore, understanding the fluid characteristic and heat transfer of the system will provide a good basis to understand the full model. Growth rate and the uniformity of the film are the two most important factors in CVD process and it is depended on the flow and thermal characteristic within the system. Optimizing the operating parameters will result in better growth rate and uniformity. Operating parameters such as inflow velocity, inflow diameter and rotational speed are used to create different design simulations. Fluid velocities and various temperatures are recorded to see the effects of the different operating parameters. Velocities are recorded by using flow meter and hot wire anemometer. Temperatures are recorded by using various thermocouples and infrared thermometer. The result should provide a quantitative basis for the prediction, design and optimization of the system and process for design and fabrication of future CVD reactors. Further assessment of the system results will be discuss in detail such as effects of buoyancy and effects of rotation. The experimental study also coupled with a numerical study for further validation of both model. Comparisons between the two models are also presented.

Acknowledgements

First and Foremost, I would like to express my sincere gratitude to my advisor, Dr. Yogesh Jaluria for the continuous guidance and encouragement throughout my master thesis. He has taught me to think beyond outside of the box. He has been a mentor not only in my academic career but also personal life. His expertise along with his patience has truly encouraged and motivated me to pursuit higher goals.

I would like to thanks my thesis committee, Dr F. Javier Diez-Garias, and Dr. Zhixiong Guo for their supportive suggestions and their time to review my thesis.

I would like thank my senior colleague Jiandong Meng for taking the time to explain all the question I have had throughout my experiment and studies. He is also been very cooperative in helping me with getting simulation data from his study.I would like to thanks Joesph Vanderveer for helping me with my experimental setup whenever I have problems and errors. He had saved me from many days of headache that I would have had.

A special thanks to John Petrowski for countless time of helping me when I was fabricating my experimental model. His vast knowledge is definitely an asset to the MAE Department. He was very patience with me and understand what I need to be done during the time he offered help.

I want to acknowledge my fiance, Katty Siu, for giving me the mental support, strength and perseverance to finish my master and pursuit higher. I am grateful to have her part of my life. And finally, I am indebted to my family for their unparalleled support for me. Thanks to all those I forgot as well.

Table of Contents

List of Figures

Chapter 1

Introduction

1.1 Introduction

Chemical Vapor Deposition (CVD) has played a huge role in many of todays modern industries. It is a widely used process that allows user to produce highly favorable material on any simple or complex surfaces. It is a heat-activated process that allows reaction of gaseous chemical compounds on a carefully prepared substrates. Microelectronics, lightings, telecommunications and energy industries growing exponentially as the CVD technology advances. Some of these growths includes highly sensitive and accurate sensors, high brightness low consumption lightings, and high efficiency photovoltaic cells. The key driving force for these advance CVD processing technique comes from companies pouring resources in research and development and the increased in government regulation for limiting energy consumptions and more demand of greener energy systems. With such a high demand in these modern advance technologies and products, it is necessary to have total controls of all variable and parameters of the CVD equipment. Even a slight change of the systems pressure, temperature or flow condition can alter the performance or structural integrity of the deposited materials.

1.1.1 Current Designs

The CVD reactor has been around for many years, and many studies have already been done to develop and improve the reactor. However, many of the reactors today still have problem of depositions, uniformity, and throughput. Horizontal reactors can produce a large volume of wafers at one time, but the problem is getting uniform deposition on each wafers. Wafers that are leading to the flow will have more deposition comparing with wafers that are at the trailing end of the flow.

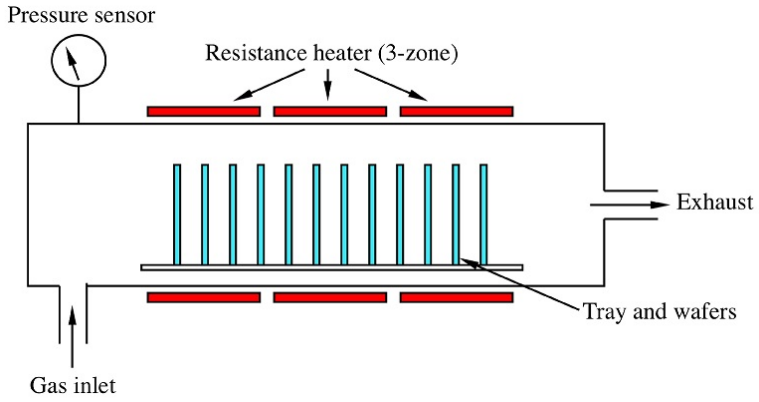

Figure 1.1: Sample Horizontal CVD Reactor. Adapted from M. Konuma [8]

Another design is the vertical impinging reactors, also known as stagnation flow reactor. It is most used type in industries today. Vertical impinging reactors can produce uniform wafer for single or low volume wafers, but when industries increase the size of the susceptor and demands for more volume, the uniformity decreases just like the horizontal reactors. Wafers near the center of the flow will have higher deposition compared to wafer located at the out edge of the susceptor. Some of the more modern CVD reactor incorporates a rotating susceptor to these two configuration for more uniformity controls, while other may include a carefully contoured flow guide to direct the flow rather than the typical vertical downward flow. For this thesis, it will be mainly focus on the vertical impinging type reactor with rotating susceptor.

1.1.2 Applications

Chemical Vapor Deposition is a very versatile process that has applications across wide range of fields. Technologies include computers, electronics, sensors, lightings, protective coatings, jewelries, telecommunications, MEMS, and photovoltaic cells. Silicon was a material used in CVD processing to produce Silicon Dioxide. It has become the game changer in the semiconductor industries. Without Silicon, MOSFET or Metal Organic Semiconductor Field Effect Transistor would not be as successful. In a typical MOSFET, there are 4 main terminal devices: Source, Gate, Drain and Bulk. The Gate

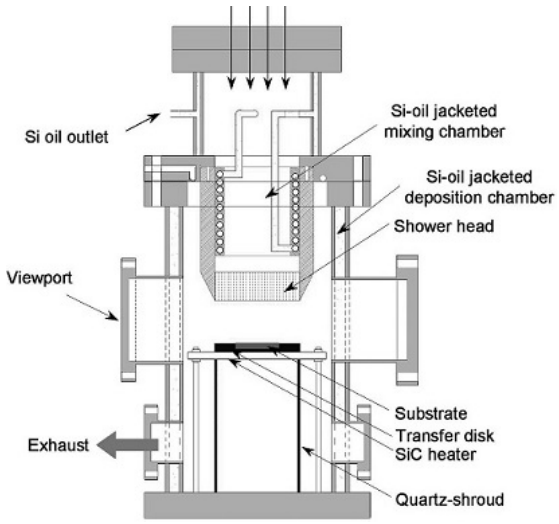

Figure 1.2: Sample Vertical CVD Reactor. Adapted from Chae *et al.* [16]

separate the channel from Source to Drain, and act as the switch of the circuit. Silicon is the material used for the Gate terminal, because of the high quality insulating layer created by the Silicon Dioxide. More recent improvement are in the optoelectronics which includes, photodiodes or photovoltaic cells, Light Emitting Diodes or LEDs, and many other Photosensors and detectors. LEDs are now the more prefer form of lighting due to its low energy consumption, longer lifetime, and overall robustness compared to other lightning source. Similar to MOSFET, LEDs are also produced by the CVD process to create the P layer and N layer on the substrate. LED is a 2 lead light source from a PN- junction diode. Photon is release when a suitable energy is applied. The color of the light is determine by the energy band gap required by the semiconductor. Using different material will target specific wavelength photon in the light spectrum. Fig. 1.3 is a chart that shows the LED colors to the corresponding material use for manufacturing.

1.1.3 Fundamentals

Chemical vapor deposition process is divided into several areas such as heat and mass transfer, thermochemistry, and kinetics of fluids and solids. For this thesis, we are focusing mainly on the heat transfer, and the kinetics of fluids. Even though it is only

	Color	Semiconductor Material
	Infrared	Gallium arsenide (GaAs)
		Aluminium gallium arsenide (AlGaAs)
	Red	Aluminium gallium arsenide (AlGaAs)
		Gallium arsenide phosphide (GaAsP)
		Aluminium gallium indium phosphide (AlGaInP)
		Gallium(III) phosphide (GaP)
	Orange	Gallium arsenide phosphide (GaAsP)
		Aluminium gallium indium phosphide (AlGaInP)
		Gallium(III) phosphide (GaP)
	Yellow	Gallium arsenide phosphide (GaAsP)
		Aluminium gallium indium phosphide (AlGaInP)
		Gallium(III) phosphide (GaP)
	Green	Gallium(III) phosphide (GaP)
		Aluminium gallium indium phosphide (AlGaInP)
		Aluminium gallium phosphide (AlGaP)
		Gallium(III) nitride (GaN)
		Indium gallium nitride (InGaN)
	Blue	Zinc selenide (ZnSe)
		Indium gallium nitride (InGaN)
	Violet	Indium gallium nitride (InGaN)
	Ultraviolet	Diamond (235 nm)
		Boron nitride (215 nm)
		Aluminium nitride (AlN) (210 nm)
		Aluminium gallium nitride (AlGaN)
		Aluminium gallium indium nitride (AlGaInN)
	White	Blue/UV diode with yellow phosphor

Figure 1.3: Table of LED color to corresponding material used

two of the many areas involved in the CVD reactor that I mentioned; it is two very important areas. But it is important to know the thermochemistry theory behind the process. As I mentioned earlier, CVD process is a heat activated chemical reaction inside a chamber to synthesize a new desired material. The temperature is very important to the deposition rate. Fig. 1.4 is the Arrhenius plot showing the dependency of deposition rate with temperature. Precursor Depletion regime occurs when the temperature is too high where buoyancy effect is high or when low inlet velocity where boundary layer is thick. It is also where chemical reaction occurs before it arrives at the surface creating powders rather than film growth. Gas phrase transport limited regime is where the deposition rate is at its highest. This regime is independence of temperature and deposition rate related to how much can the system delivery precursor gas into and out of the chamber. Difference precursor gas has different temperature ranges for this regime. For silicone epitaxial growth, it is range between 1990 - 2100°C and for GaN epitaxial growth is 1400-1600°C. Last regime is surface reaction limited regime and it occurs when temperature are too low. Chemical reaction cannot take effect when there

are not enough thermal energy to break them apart and it would be a waste of resources as gas will just enter and exit the chamber. When the temperature is just right, the chemical reaction occurs on the surface of the substrate. A substrate is where the new material structure is grown on. The substrate also act like a seed for crystalline growth, so to get a certain crystalline structure you would need a specific cut of the substrate. For epitaxial growth, where all atom are lined up and layered, you would need a certain Miller index substrate. AlN 0001 epitaxial growth need Al (111) substrates.[14] For CVD processes, sapphire and silicon are often use as substrate.

1.1.4 CVD Process

CVD starts its process by the used of gases and vapors. Since there are combination of gases and vapors present inside the chamber, it is also important to know the properties and the flow characteristics of the materials. There are 4 type of gases used in a CVD reactor: Precursor, Carrier, Reactive, and Dopant. Precursor gases are the raw materials such as Silane or SiH_4 and the outcome would be silicon dioxide. Raw material that are not in gaseous form will undergo a phase change before entering the chamber. Liquid materials such as Trimethylgallium (TMGa) will be placed in a temperature controlled apparatus called bubbler to convert the liquid form into a vapor form. Both gaseous and vapor state material is transported into the chamber by the carrier gas. The sole purpose of the carrier gas is to transport other gases and vapor into and out of the chamber. Typical carrier gas used are Nitrogen (N_2), or Argon (Ar) due to their inert characteristics. Reactive gas reacts to the precursor gas to produce the desired material. The new material is a crystalline film structure that is formed on the surface, and as more reaction occurs the faster the growth of this thin film. Last type of gas is called Dopant. As more and more complex materials are used, the more byproduct it will produce in the system and some of these byproduct are radicals molecule that will reacts to other material causing impurities in the film growth. Dopant gases are used to neutralize these radicals molecule to promote growth rates of desired materials.

Chemical reaction only occurs when the system has enough energy, and this energy is fuel by the heat transfer that occurs between the heaters and the chamber. Some of

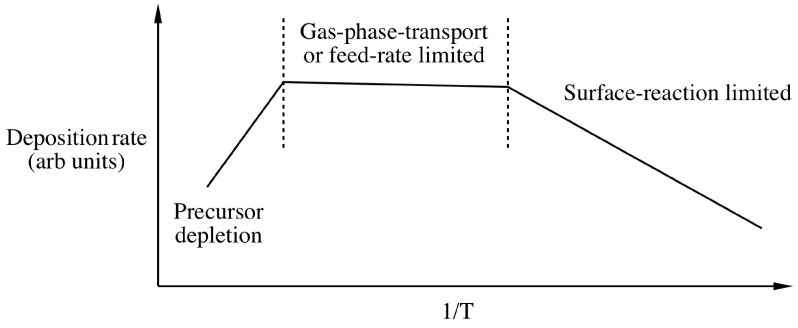

Figure 1.4: Dependency of deposition rate with temperature. Adapted from J. G. Eden. [6]

these heater source can be microwave heating, induction coil heating or resistive heating. As the chamber heats up to the desired temperatures, the precursor gas and the reactive gas molecules begin to break apart from the surrounding thermal energy or adsorpton phase. After molecules are in their radical forms, they react with other radicals and recombines to form the new materials. This is the reaction phase and it occurs usually near the substrate surface. Concurrently, excessive byproducts and energies are release from the new materials back into the freestream. This is the desorption phase. The new material is deposit on to the substrate and it begins to grow in thckness as more and more chemical reaction occurs. The byproduct exits the chamber as more precursor and reactive gas enters the chmaber. The pressure and flow rates of these chemical during the process plays an important role in controlling uniformity and growth rates. Almost all CVD reactors follow these steps. Fig. 1.5 illustrate the CVD process for Silicone Dioxide SiO_2 from using Siliane SiH_4 as the precursor gas and Oxygen (O_2) as the reactive gas.

The precursor gases falls under one of these categories. First type is called Halides, this chemical group contains one part halogen atom such as Sodium Chloride (NaCl) or Titanium Tetrachloride ($TiCl_4$). Second type are called Hydrides. This group of metalloids contains hydrogen in the compound such as Silane (SiH_4) or Ammonia (NH_4). Third type are called Metal Organics groups. This type split into more known sub

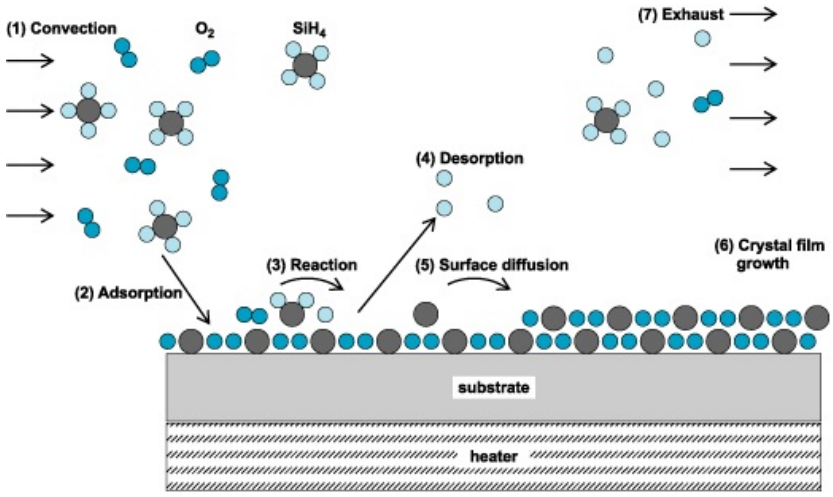

Figure 1.5: Detail CVD process for silicon from precursor gas Silane (SiH_4).

categories called Alkyls, Alkoxides, and Carbonyls. Alkyls are alkane missing one hydrogen atom such as methyl (CH_3). Alkoxides are metal organic group bounded to a negatively charge oxygen atom. It is usually produce from an alcohol group. Carbonyls are molecules that contains a carbon atom double bonded to an oxygen atom with other transitional metal. Currently there are many chemicals that can be deposit by the CVD process and each precursor material is chosen based on material property, decomposition temperatures, vapor pressure of the precursor gas, safety and the cost of the material. Fig. 1.6 shows all the materials that has been deposited by CVD process.

PERIODIC TABLE

IA	IIA	IIIA	IVA	VA	VIA	VIIA	VIII			IB	IIB	IIIB	IV	VA	VIB	VIIB	O
1 H 1.008																	2 He 4.003
3 Li 6.941	4 Be 9.012											5 B 10.81	6 C 12.01	7 N 14.01	8 O 16.00	9 F 19.00	10 Ne 20.179
11 Na 22.990	12 Mg 24.305											13 Al 26.98	14 Si 28.09	15 P 30.97	16 S 32.07	17 Cl 35.45	18 Ar 39.948
19 K 39.098	20 Ca 40.08	21 Sc 44.956	22 Ti 47.90	23 V 50.942	24 Cr 51.996	25 Mn 54.938	26 Fe 55.847	27 Co 58.933	28 Ni 58.70	29 Cu 63.546	30 Zn 65.39	31 Ga 69.72	32 Ge 72.61	33 As 74.92	34 Se 78.96	35 Br 79.90	36 Kr 83.80
37 Rb 85.468	38 Sr 87.62	39 Y 88.906	40 Zr 91.22	41 Nb 92.906	42 Mo 95.94	43 Tc (99)	44 Ru 101.07	45 Rh 102.905	46 Pd 106.4	47 Ag 107.868	48 Cd 112.4	49 In 114.8	50 Sn 118.7	51 Sb 121.8	52 Te 127.6	53 I 126.9	54 Xe 131.30
55 Cs 132.905	56 Ba 137.33	57 La 138.9	72 Hf 178.49	73 Ta 180.948	74 W 183.85	75 Re 186.2	76 Os 190.2	77 Ir 192.22	78 Pt 195.09	79 Au 196.966	80 Hg 200.59	81 Tl 204.37	82 Pb 207.2	83 Bi 209.0	84 Po (210)	85 At (210)	86 Rn (222)
87 Fr (223)	88 Ra (226)	89 Ac 227.0															

LANTHANIDES	57 La 138.5	58 Ce 140.115	59 Pr 140.1	60 Nd 144.2	61 Pm (145)	62 Sm 150.4	63 Eu 152.0	64 Gd 157.2	65 Tb 158.5	66 Dy 162.5	67 Ho 164.5	68 Er 167.2	69 Tm 168.5	70 Yb 173.0	71 Lu 174.96
ACTINIDES	89 Ac 227.0	90 Th 232.0	91 Pa 231.0	92 U 238.0	93 Np 237.0	94 Pu (244)	95 Am (243)	96 Cm (247)	97 Bk (247)	98 Cf (251)	99 Es (252)	100 Fm (257)	101 Md (256)	102 No (259)	103 Lr (257)

Figure 1.6: Shaded element indicates it has been deposited by CVD. Adapted from Creighton et al. [3]

Chapter 2

Objectives

2.1 Motivation

The current technology behind Chemical Vapor Deposition can definitely be improve. Many CVD related industries still faces numerous problems in the manufacturing process. Uniformity and growth rates are still issues that need to be improved on. As industries step up to produce larger wafers, 4 inches and larger, the uniformity and quality of the wafer decreases. Even for the smaller wafer designs, industries has been using excessive raw material to yield satisfactory level of output. It is important to optimized the used of raw material to keep the cost down for consumers. Our motivation for this thesis is to start probing the fundamental theory behind Chemical Vapor Deposition. By understanding the flow characteristic of the flow and heat transfer inside the chamber, we can accurately model the chamber by computational method. Industries spent thousands of dollars on raw materials by trial and error to get adequate results. If computational model are as accurate as the reactor, finding the optimal growth rate and best uniformity would cost only computational time. For this study, a simple experimental model was created to mimic an atmospheric rotating vertical impinging chemical vapor deposition reactor. We looked into many operating conditions to see the effect of each parameter such as the effect of rotation, and the effect of buoyancy.

2.2 Literature Review

Another motivation was Nasir Memon's Master Thesis in 2009. We want to continue the study that was started by Memon by incorporate a rotational susceptor, and comparison study to a computational model. During his study, he looked into an impinging jet CVD

reactor, where he wanted to create model that help "... develop models that predict flow patterns in such a reactor to achieve a uniform deposition across the substrate." [9] He also preform numerous case studies on buoyancy effect for the standard reactor configuration, where the results for "... mixed convection value of 0.96, with inlet velocity of 0.11 m/s, buoyancy significantly impacts the inlet flow, which will lead to an uneven deposition across the substrate." [9] He concluded that CVD can be operated in atmospheric conditions given the limitation of buoyancy force and the specific operating conditions.

Chiu *et al.* did a study of heat transfer in a horizontal channel with a heated section. The model stimulated a horizontal CVD reactor chamber where air was flowed from one end of the chamber and exits the other end. When the heater was on, the flow near the heated area becomes disturbed by the plume created by heater due to buoyancy effect. It generated recirculation or roll inside the channel. "These rolls can have significant altercations to the surface temperature and heat transfer rates." Chiu also states that "...deposition rate and film uniformity can be affected by the convective displacement of reactants." Further into the investigation, numerical study of the heated channel was also done. Chiu was able to validate the experimental results with numerical data. He was able to numerically predict operating conditions by changing the systems material using his model. Comparison of experimental results with numerical predictions show good agreement. [2]

Xenidou *et al.* created an experimental Metal Organic Chemical Vapor Deposition (MOCVD) reactor to study the growth of Aluminum films. In his study, a shower head deposition was created with no flow guide and no rotational effect. He was able to gather results of temperatures and flow profiles using thermocouples, mass flow controllers, and pressure measuring device. "The model was found to predict, fairly well." [15] However, Xenidou was unable to capture the effect of buoyancy because the low dissociation temperature range for Al deposition. "Al growth through DMEAA dissociation is investigated in the temperature range of 473-493K, where the growth takes place in the transport-controlled regime" [15] Xenidou also did a Richardson numbers study and found that to be 0.115, where force convection parameter dominates

the buoyancy effect. Lastly, the lack of a rotational susceptor indicated that flow altering method is not necessary in this case, as recirculation due to buoyancy force is negligible. Concurrently, he created a computational with operating conditions similar to the experimental model. At the end, he was able to show the similar trend between the experimental and computational model.

Terai, *et al.* investigated the high speed rotating disk CVD process for silicon films and they are trying to find a solution to growing high quality and high productivity films. Terai states that "Good thickness uniformity, few particles, and a high deposition rate are necessary for high productivity." The reactor they are using for this studies has many controllers and sensors for operating condition monitoring. Terai was able to run their reactor up to rotational speed of 3,000 RPM and temperature reaching to 720°C. With that temperature, buoyancy effect was dominate even if the reactor pressure is at a low pressure of 50 Torr. Terai also shows that rotational speed effect the uniformity. "The simulated thickness of the boundary layer drastically decreases with rotational speed, and approaches 10mm at 3000 rpm" [11]. We know that thick boundary layer causes flow separation and buoyancy effect increase this effect. Keeping the boundary layer small will reduces recirculation that cause uniformity problems.

2.3 Present Work

There are many studies about chemical vapor depositions especially with specific materials and computational models, but very limited investigation in experimental study of the rotational reactors. The present work involves an experimental study in a rotational reactor at atmospheric pressure. Air will be used as the material to conduct the study of the temperature profiles and flow characteristics inside the reactor. Altering the flow inside a highly buoyancy reactor by inducing a rotational effect will yield a more favorable film growth conditions. Understanding these parameters will aid in developing model that can predict operating conditions for different type of crystal growth more efficiently. Computational model that was validated with experimental result shows a more similar results than just computational studies alone.

Chapter 3

Experimental Setup

3.1 Introduction

An experiment model was set up to investigate the flow characteristic and heat transfer inside a vertical rotating impinging chemical vapor deposition reactor. This is a simple model that consists of a vertical rotating susceptor powered by a variable speed drill motor and controller. Flow meter, pressure valve, and hot wire anemometer is equipped to measured outlet velocities and temperature. Thermocouples were installed to measure susceptor and reactor temperatures. All connected to a Data Acquisition (DAQ) system for future data analysis. Fig. 3.1 shows the general setup of the experimental setup.

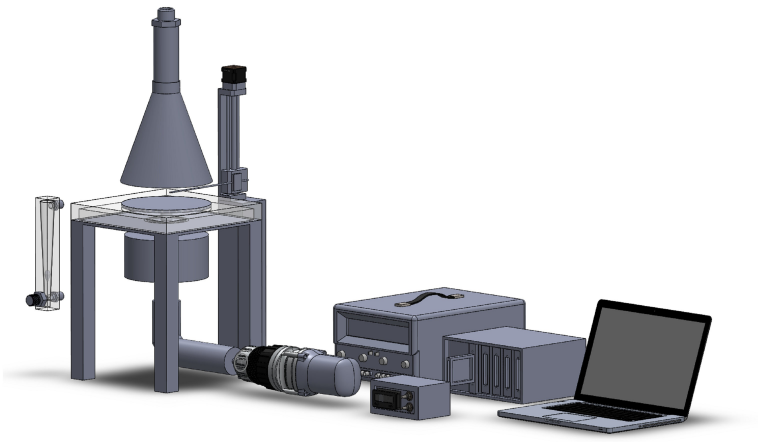

Figure 3.1: Experimental CVD reactor setup

3.2 Equipment and Measurement Devices

3.2.1 Main Model

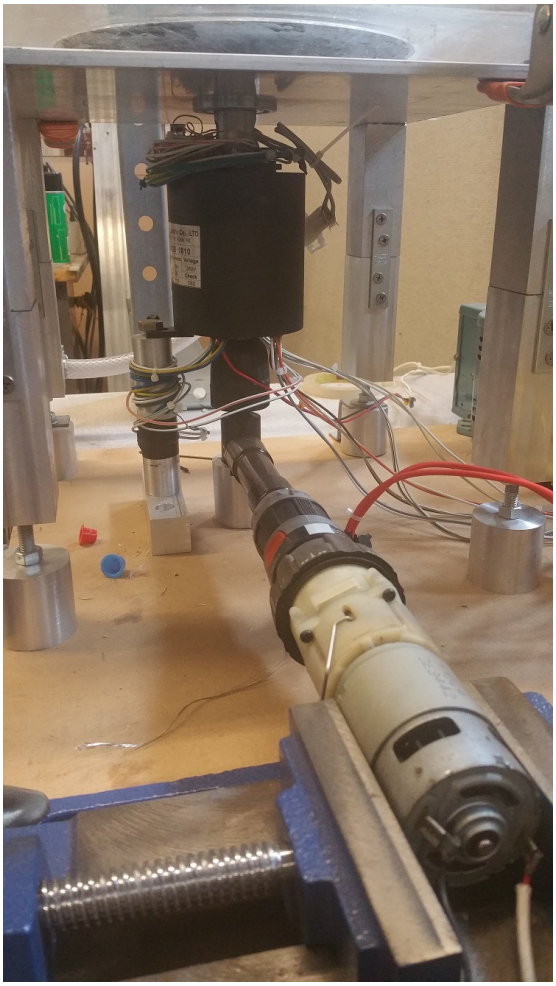

Figure 3.2: Image of the lower platform

The experimental model consists of a stationary platforms, a heated disk plate and a flow guide. The lower stationary platform is constructed from a 6.35mm thick 6061 Aluminum plate. It is measured 304.8mm by 304.8mm. A sealed roller bearing was pressed in at the center for the rotating mechanism. The interior diameter of the roller bearing is measured to be 25.4mm. Platform was measured to be 279.4mm high and it is bolted down to the table to restrict movement and vibration when the disk is in motion. A 25.4mm diameter hollow row that is connected to the rotating plate is

placed thru the roller bearing. It is hollow rod for the purpose of wiring connections and reducing the heat conduction from the disk into the rod. The rotating disk is also made from 6061 aluminum and it is 203.2mm in diameter and 6.35mm thick. The other end of the hollow rod is connected to a 1:1 right angle drill attachment. This will allow the motor and transmission can be mounted horizontally for the purpose of reducing the total height of the platform. Fig. 3.2 shows an image of the lower platform and Fig. **??** shows an image of the right angle drill attachment

Figure 3.3: Enlarged view of the right angle drill attachement

Connecting to the right angle drill attachment is the variable speed drill motor paired with a 30 amp pulse-width modulation (PWM) motor controller. PWM controllers converts digital signal into an analog signal. In simple terms, it is a voltage regulator. The controller will send power from the battery to the drill motor at a specific duty cycle. The drill motor and transmission is taken out from a 18 volt Black and Decker drill. It is rated up to 1,200 rpm with 2 transmission settings. Low gear for a more accurate low rpm control and high gear for more accurate high rpm controls. Fig. 3.4 shows an image of the drill motor and transmission and Fig. 3.5 shows an image of the PWM controller.

Figure 3.4: 18 volt drill motor and transmission

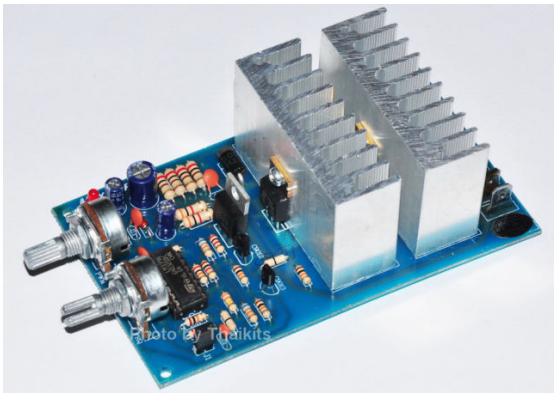

Figure 3.5: Pulse Width Modulation Control Board

An acrylic upper platform is place on top of the aluminum platform to have an even surface with the disk. Acrylic was chosen because its less heat conductive than aluminum so heat transfer from the side of the disk can be minimize. The flow guide is placed above the rotating plate and acrylic platform. Its a cone shape guide with the bigger diameter measuring 203.2mm, same as the diameter of the disk. A long PVC tube is connected to the inlet of the flow guide. The tube is 50.8mm in diameter and 609.6mm long. It is served as flow straightener as the air flows onto the plate. The tube can also be adapted to have a smaller inlet diameter of 25.4mm by inserting a 25.4mm tube inside the 50.8mm tube. An Omega Rotameter and pressure regulator is used to control the compressed air before going into the flow straighter tube. Fig. 3.6 shows the setup of the upper platform with the flow guide.

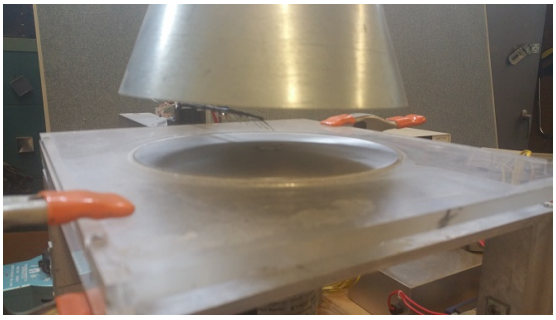

Figure 3.6: Image of the upper platform and flow guide

3.2.2 Flow regulator

An Omega rotameter and generic pressure regulator is used to control the compressed air before going into the flow straighter tube. Pressure regulator has a 0-1,380 kPa pressure range to control incoming pressure. After the flow regulator, an Omega rotameter was also used to regulate volume flow rate into the chamber. It is an acrylic style rotameter for air measure. The model that is used is Omega FL4513V, and it has an 8 SCFM max air flow with a valve. Max pressure rated is 100 PSI and max temperature of 38°C. The accuracy of this rotameter is ±3 SCFM. Fig. 3.7 shows image of the Omega rotameter.

Figure 3.7: Omega Rotameter

3.2.3 Heater System

The bottom of the rotating disk is heated by 312 watt heating cable, capable reaching 760°C. It uses a 120 volt plug with a 2.6 amp draw. The heating cable is 12.7mm in diameter and 1.83m long. The heating element is manufactured by HTS/AMPTEK. It is a heavy AMOX insulated duo-tape heater. The calculated heat flux into the plate is 9,621 W/m^2. The heater is molded onto the bottom side of the plate, secured by layer of Cotronics Resbond 907 fireproof adhesive and sealant. It is then insulated by heat-resistance mica glass-silicone infused wrap, and a layer of fiberglass cloth to reduce heat loss from radiation and convection under the plate. A variable transformer

was used to control the power going through the heater. The device is made by Staco Energy. It has a 120V input and 0-120V output with 10A maximum current. Fig. 3.8 shows an image of the variable transformer. Fig.3.9 shows an image of how the heater get embedded onto the plate.

Figure 3.8: Staco Variable Transformer

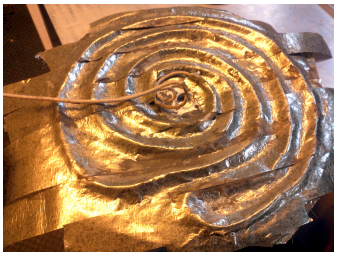

Figure 3.9: Heater Plate Assembly

3.2.4 Thermocouples

Thermocouples are fabricated in the laboratory by the use of Hot Spot thermocouple welder. Chromel-Alumel or type k thermocouple wires are used in this experiment. Positive electrode are made from 90 percent nickel and 10 percent chromium, while the negative electrode consist of 95% nickel 2% manganese, 2% aluminum, and 1%t silicon. The wires are 30 American Wire Gauge (AWG) and 0.5mm in diameter. Type K thermocouple has a error of $\pm 2.2°C$.

The Hotspot TC welder is powered by an AC line through a step-down transformer. It will generate an electric arc for fusing individual thermocouple leads into freestanding bead. Welding power is adjusted by a control knob ranging from 5 to 50 watt second and power requirement for thermocouple is determine by the wire size and material of the thermocouple wires. In this experiment, the control is set between 18 to 22 watt second ranges. To perform the weld, the wire are held on the attached pliers and set in contact with the carbon electrode. A switch is depressed to create the arc weld that fuses the two metals together. Fig. 3.10 show an image of the HotSpot Thermocouple Welder. Fig. 3.11 shows an image of the lab fabricated thermocouple.

Figure 3.10: Hot Spot Thermocouple Welder

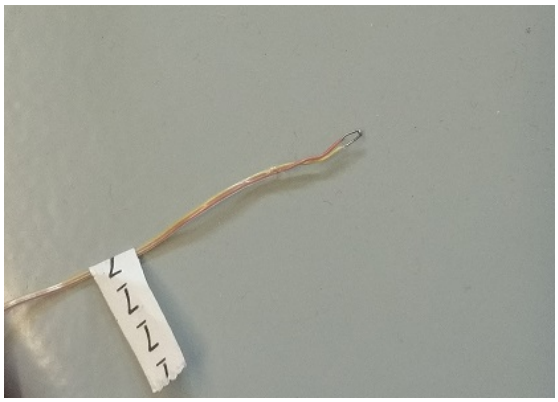

Figure 3.11: Lab Made Thermocouple

3.2.5 Slip Ring

A slip ring is an electromechanical device that allows transmission of power and electrical signal from a stationary structure to a rotating structure. The contacting point consists of brushes and slip rings. Where the brushes are on the rotation side and the rings are stationary. As the structure rotates, the brushes keep constant contact to the slip rings. Each brush and slip ring is considered as 1 circuit or 1 connection. The one used for this experiment was from KEYO Electric. It is an 18 connections through-bore type slip rings module, with 10A maximum amperage and 380v maximum voltage. The 18 connections will give us 9 channels to use for power and signal transmission. It is recommended by the manufacturer to have empty channels between the power and signal channels to reduce interference and noise to the channels carrying signals. The center bore is 25.4mm for fitting the drive shaft that connects to the heater plate. It can hold electrical current and signals up to 1000 RPM. Image of the slip ring is shown in Fig. 3.12.

Figure 3.12: Keyo Slip Ring - 25.4mm thru bored, 18 connections

3.2.6 Hot Wire System

The hot wire anemometer system is attached to the platform outside of the disk. It will measure exit velocity and exit temperature. This system has velocity range of 0.1-25 m/s with an accuracy of ± 0.1 m/s. The temperature range is from 0-50°C with an accuracy of ± 1°C. The image of the portable hot wire system is shown on Fig. 3.13

Figure 3.13: Portable Hot Wire Anenometer

3.2.7 Tachometer

The disk rotation speed is recorded manually by a non-contact tachometer made by Mitutoyo. Its range of measure is 6 - 99,999 RPM with accuracy of 0.006 percent and 0.5 digit. The reflective sticker was placed on the outside edge of the plate. The measuring device is aligned straight above the reflective sticker for proper measurement. Fig. 3.14 is an image showing the tachometer.

Figure 3.14: Non-Contact Laser Tachometer

3.2.8 Infrared Thermometer

The thermocouples used are unshielded and when it touches with a metallic surfaces, readings becomes inaccurate. Therefore non-intrusive infrared thermometer is used for measuring surface temperatures. The one used is manufactured by Amprobe. Its range is from -32°C to 1050°C with accuracy of ±1.8°C. The thermometer is programmed with emissivity of 0.15 for oxidized aluminum. An image of the infrared thermometer is shown on Fig. 3.15.

Figure 3.15: Infrared Thermometer for Surface Measurement

3.2.9 Data Acquisition (DAQ) System and Software

The DAQ system consist of National Instruments (NI) Input-Output Motion controller, National Instruments signal acquisition system for thermocouples, and a hot-wire anemometer system. There are two other measuring devices that data are manually recorded such as rotational speed, and plate surface temperature. These measuring devices are non-intrusive. The NIs UMI-7764 Input and Output Motion Controller was setup for the use of motion of the thermocouple inside the CVD reactor. Eight (8) thermocouples are placed above the disk to measure flow temperature as it moves away from the heated plate. The linear motion is controlled by the Velmex XSlide system with a Vexta NEMA 17 two phrase stepper motor. The motor can move 0.9° per step and 400 steps per revolution. It has 6 leads coming from it: red, white, blue, black, yellow and green. The two phase motor indicated that it can run in unipolar mode or bipolar mode. Unipolar mode, the motor can run at higher winding speed but lower torque to hold the stepper in place. While in bipolar mode, the motor has a higher torque but lower winding speed. For unipolar, the 6 wires are configured as a H- bridge. In Bipolar mode, the center tap leads are left disconnected. Fig. 3.16 show an image of the stepper motor, and Fig. 3.17 shows an illustration of the stepper motor's wiring.

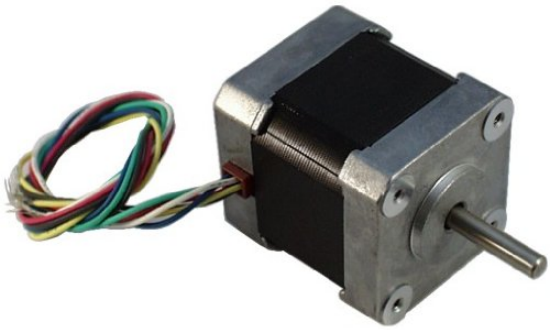

Figure 3.16: NEMA 17 Stepper Motor

Wire Color	Connection
Black	Phase A
Green	Phase $\overline{A}$
Yellow	Phase A-CT†
Red	Phase B
Blue	Phase $\overline{B}$
White	Phase B-CT†

† CT stands for Center Tap

Figure 3.17: Wire lead pinout

The stepper motor is connected to the Velmex Xslide Linear Actuator. Linear actuator is a mechanical device that converts rotational movement into linear movement. This particular one is a screw type actuation where the rate of the linear motion depends on the screw pitch. This actuator is equipped with a screw pitch of 0.635mm per revolution. It can travel total distance of 304.8mm. The system also has a built in limit switch on the two ends of the actuator. When the platform hits the switch it cuts off power to prevent screw damage. Combining the specification from the stepper motor, the step it takes to move 25.4mm in distance is 16,000 steps. An image of the Xslide is shown on Fig. 3.18

Figure 3.18: Stepper motor and Velmex Xslide system

The motion of the Xslide is controlled by National Instrument UMI -7764 motion controller. It is a device that links the communication between the LabView Data

Acquisition Software to the motor. The motion controller has a built in inhibit logic that can control 4 different axis. This unit also allow the use of 3rd party motor drivers. The motor driver received the signal from the motion controller, and sent out current from a power supply into the motor. The driver also reads the step signal from the stepper motor and relay it back to the motion controller. Hence, stepper motor are very accurate in controlling the movement of the spindle. An image of the UMI-7764 motion controller is shown on Fig. 3.19.

Figure 3.19: National Instrument Motion Controller

There are eight thermocouples above the heat plate and as well as five embedded thermocouples inside the plate. The five embedded thermocouples are located at the center of the plate. It is connect to a slip ring connection, since the five thermocouples are going to be in motion with the plate. The stationary part of the slip ring connection, along with the eight thermocouples, is connected to the NIs signal acquisition system, capable of 32 channels at ± 10 volt analog input. The system consists of SCXI chassis, with SCXI input module, and a thermocouple terminal block.The chromel-alumel or type K thermocouples have the range of -200°C to 1350°C which is within the range of measure for this experiment. The SCXI system is shown on Fig. 3.20.

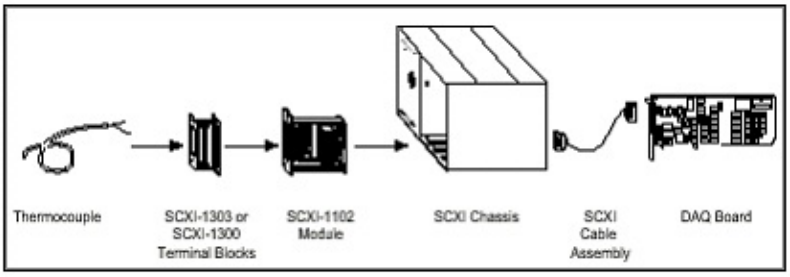

Figure 3.20: Schematic of the NI's SCXI system

National Instrument's SCXI-1000 chassis has ability to house 4 different SCXI modules. The device has built in timing circuitry for high speed multiplexing data gathering. This is the main device that powers the modules and provide the data communication between the DAQ card inside the computer and the modules via a special NI cable. In this setup, we are only utilizing one module. The SCXI-1102 is the module that is being used in this setup. The SCXI-1102 is specifically designed for high accuracy temperature measurements via thermocouples. This module includes a 32 channels that can acquire many different signals. SCXI-1300 terminal block is required to attach to the SCXI-1102 to allow thermal couple leads connections. This terminal block link them to other module for data recording or data processing. It can also connect to an user Interface modules for monitoring and controlling abilities. These user interface module includes displays, switch, knobs, graphs, meters and gauges with is shown on the front panel. The front panel is where graphical interface is located. On this screen, you only see things you would see in front of a device such as a switch, meter or gauges. This is where you would monitor the system. The block diagram is where all the virtual wiring and modules are located, and front panel is where user can monitor or control the devices. For this setup, we set up a graph showing temperature vs. time and a display output for each channel. Data is also recorded to a file saved at a designated location. A screenshot of the LabView's front and block panel is shown in Fig. 3.21 and Fig. 3.22 respectively. The programing is very straightforward. Get the signal from the DAQ hardwares, split into 2 output. One outputs to the front panel for the user to see via graph and numerical readout. The second output saves all the reading onto a

file for further data analysis. For the motion control, we used a built in software that came with the motion control package. The program was tweaked to accommodate the stepper motor and linear actuator. Stepper motor activates by inputting the number of steps the user wants. Positive number for a clockwise direction and negative number for a counter-clockwise direction.

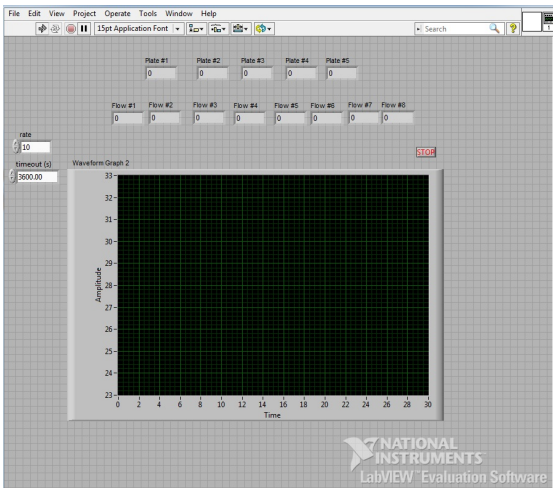

Figure 3.21: LabView Front Panel

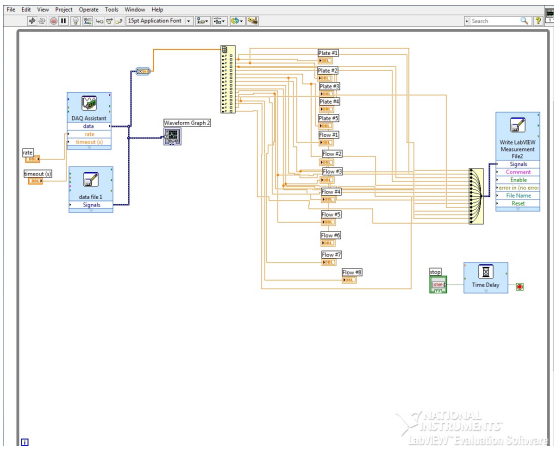

Figure 3.22: LabView Block Diagram

3.2.10 Fog Machine

The Rosco Alpha 900 Fog Machine is used for flow visualization purpose. It is connect to the top of the flow straighter and activate with the remote when needed. The machine has a 1000 watt heater system and large storage tank for the smoke generating liquid. It is powered by 110v outlet and it is turned on via main switch on the rear of the machine. The remote controller activate the fog and it is a simple push button switch that turns on the machine when you hold the switch to on position and turns off when you let go of the switch. An image of the fog machine is shown in Fig. 3.23.

Figure 3.23: Fog Machine for flow visulization

3.3 Experimental Procedures

This section will describe in detail of the experiment procedures.

1. Turn on computer and systems hardwares
   (a) SCXI system for thermocouples
   (b) NI motion controller
   (c) Power supply for stepper motor
   (d) Power supply for stepper motor driver
   (e) Power the drill
   (f) Power the heater and set to 0% duty
2. Start NI Measurement & Automation Explorer software
   (a) Initialize stepper motor and drivers
3. Start LabView Program and motor controller program
4. Purge airline to get rid of moisture
5. Turn on air supply and set desire pressure and flow rate
6. Increase the heater duty to 50% or 100%

7. Wait until temperature of the plate stabilized (30 min)
8. Set rotational speed with PWM controller and tachometer
9. Make sure flow thermocouple are at 0 position
    (a) if not, set to 0 position (right above the plate but not touching the plate)
10. Use infrared thermometer to record surface temperature
11. Press start on the LabView program and wait for 30 second.
12. Stop the recording, and set the next stepper motor position (500 steps/increment)
13. Wait until temperature stabilized on the monitor screen ($\pm 0.2°C$)
14. Repeat recording until, 20 increment has been made.
15. Record rpm, inlet diameter, inlet velocity, and exit velocity
16. Once the experiment are finish
    (a) Turn off heater and set duty to 0%
    (b) Turn off rotation and power down drill motor.
    (c) Turn air source to full flow to cool down the heated plate.
    (d) Power down power supply to stepper motor and driver.
    (e) Once the plate thermocouple temperature reaches room temperature on the monitor screen, turn off air supply
    (f) Save all data, and close LabView and motor controller software.
    (g) Power down SCXI and NI motion system

Chapter 4

Validation and Verification

4.1 Introduction

Each and every day, human accepts some degree of errors of some sort. It can be in the form of monetary round off error when dealing with money or dimensional error when buying a shoe or pants that almost fits. We dont realize it but everything in the world has errors. What is important is how much error it takes until it is unacceptable. Human knows that everything and anything cannot be perfect, therefore we allow errors within a certain range. This range is called uncertainty and within this range lies the true value or the number that we called perfect. The smaller the range the more confident you can say that "this is prefect," and this specific range is called confidence interval. A 95% confidence interval means that your range of error is only 5% from the perfect or true value. In many applications, confidence interval of 95% or better are usually accepted and anything below 95% will be rejected. This specific allowable range we called standards. Many industries created standards where allowable or tolerable range is carefully stated. Any value outside of this range will be rejected because error greater than allowable means greater chance of failure of the system.

4.2 Precision and Bias Errors

For experimental lab work, there are also errors when we collect data. This errors can be from humans, the surroundings, uncontrollable disturbances or it can be from the equipment. Human errors and errors due to surrounding are called Precision or Random Errors. "The precision of a measurement process refers to, and is determined by the degree of mutual agreement characteristic of independent measurements of a single

quantity yielded by repeated applications of the process under specified conditions." [7] Errors from equipment and resolution are called Bias or Systematic Errors. "...Systematic error is used to cover all those errors which cannot be regarded as fortuitous, as partaking of the nature of chance. They are characteristics of the system involved in the work; they may arise from errors in theory or in standards, from imperfections in the apparatus or in the observer, from false assumptions and etc.. They are frequently called constant errors, and very often they are constant throughout... " [5]

Precision and Bias Errors can be combines and express in term of uncertainty. For a specific measurement x, we can denoted the Bias Error as B_x and the Precision Error as P_x, then the total uncertainty U_x of the system can be found by the follow equation:

$$u_x = \sqrt{B_x^2 + P_x^2} \tag{4.1}$$

This value u_x is for a single measurement. If there are multiple measurement, then you would have a u_x for each and every measurement. If the standard unit of the uncertainty is the same for every measurement, then the combined uncertainty u_y is the root mean squared of all the uncertainty. This is used to determine the propagation of the errors. This formula is given by the following.

$$u_y = \sqrt{u_1^2 + u_2^2 + ... + u_n^2} \tag{4.2}$$

However, if the units are not in agreement then u_y is given as:

$$u_y = \sqrt{\left(\frac{\partial y}{\partial u_1}u_1\right)^2 + \left(\frac{\partial y}{\partial u_2}u_2\right)^2 + ... + \left(\frac{\partial y}{\partial u_n}u_n\right)^2} \tag{4.3}$$

4.3 Dimensionless Numbers

Dimensionless numbers are bare numbers that gives a quantify representation of a physical characteristic. Often it is an expression of a ratio of 2 or more parameters and the physical units are canceled thus giving a dimensionless numbers. Since the number has no units, it can be applied to all physical characteristics of any forms. Parameters

can be broken down to these 3 traits: Geometric similarity, kinematic similarity, and dynamic similarity. Geometric similarity are when the model and prototype are similar in the length scales. The proportion of each of the 3 dimension in all coordinate are scale to a constant number. Kinematic similarity are when the direction and magnitude are scale to a constant scale factor. Dynamic similarity are when all physical characteristics are scaled to a constant number. The prototype and model have the same length scales, time scales and mass scales. For this study, we are focus on the fluid dynamic and heat transfer related dimensionless numbers.

4.3.1 Normalized Terms

Normalized length and temperaure is used in this study as a length and temperature scale. It is called normalized because the highest value is 1. Normalizing the length will put the dimension in terms of the largest length in the system. For this study, we will be using 2 normalized length: one respect to the height and one respect to the radius. Normalize temperature is used in a similar way as the normalized length. Normalizing the temperature will show a comparison of temperature with respect to a reference temperature. It takes away the variation of taking a temperature inside a cold room or a hot room. We can neglect the errors from these terms as they are small relative to the other errors.

$$y^* = \frac{y}{H} \qquad (4.4) \qquad r^* = \frac{r}{R} \qquad (4.5) \qquad \theta = \frac{T - T_\infty}{T_{avg} - T_\infty} \qquad (4.6)$$

4.3.2 Reynolds Number

Reynolds number is highly used in the fluid dynamic field. It is the ratio of inertia forces and viscous force. This numbers tells if the flow is in a laminar regime or turbulent regime. For a flow through a tube, the equation is given as:

$$Re_{inlet} = \frac{4Q_{inlet}}{\nu \pi D_{inlet}} \qquad (4.7)$$

Where Q_{inlet} is the volumetric flow rate into the system, D_{inlet} is the inlet diameter,

and ν is the kinematic viscosity of the fluid. In a pipe, flow becomes fully turbulent when Re is greater than 2,300. Error propagation of this Reynolds number are from the flow rate, kinematic viscosity, and the inlet diameter. Flow rate is taken by the rotameter which has an error of ±3.5% at fill scale. Bias error from diameter found to be ±1% and bias error from kinematic viscosity is found to be ±1% as well. [1] Overall errors in Reynolds number is calculated to be ±3.77%

We also need to consider one additional Reynolds number, and that is the Reynolds number from rotational flow and it is given as:

$$Re_{rotation} = \sqrt{\frac{\omega r_{disk}^2}{\nu}} \tag{4.8}$$

Where ω is the RPM for the disk, r_{disk} is the radius of the disk at the measuring position and ν is the kinematic viscosity of the flow. Flow becomes fully turbulent when Re becomes above 10,000. Error Propagation from this Reynolds number are from the rotation speed, diameter of disk and the kinematic viscosity. RPM is taking from a tachometer which has an error of 0.006 percent. Errors from disk diameter was ±1% and errors from kinematic viscosity is found to be also ±1%. Overall errors in rotational Reynolds number is calculated to be ±1.41%

4.3.3 Grashof Number

Grashof number is an important dimensionless number for heat transfer. It is a ratio between thermal buoyancy force with viscous forces. It is given as:

$$Gr = \frac{g\beta(T_{surface} - T_{\infty})D^3}{\nu^2} \tag{4.9}$$

Where g is Earths gravity, β is the thermal expansion coefficient, D is diameter of disk, and ν is the kinematic viscosity. Error propagation from this number are from diameter of the disk, the kinematic viscosity and temperatures measurements. The disk and the kinematic viscosity is to be found as ±1% as stated previously. Thermocouple errors is given as ±0.75%. Total error from Grashof number is calculated to be ±1.6%.

4.3.4 Richardson Number

Richardson number is a ratio between the Grashof number and the Reynolds number. This numbers tells if the flow is experiencing buoyancy effect or when buoyancy forces are negligible. If the It is given as:

$$Ri = \frac{Gr}{Re^2} = \frac{\text{Natural Convection}}{\text{Forced Convection}} = \frac{Gr}{Re_{inlet} Re_{rotation}} \tag{4.10}$$

Where Gr is the Grashof number and Re is the Reynolds numbers. We will be using Reynolds number from both the inlet term and the rotational term to analyze the convection characteristic in the system. Combining the error propagation from the above terms gives us an error for Richardson number is calculated to be $\pm 4.33\%$

4.4 Calibrations

Calibration is the process of standardizing the measurement sensor. To reduce bias errors, calibration is necessary for all experimental work. For this study, many of the instrument are auto calibrated before use, such as the tachometer, and hotwire sensors. However, the thermocouples are require to be calibrated before it can be used accurately. LabView has a built in calibration feature that calibrates this type of thermocouple. To calibrate, we need to find 3 standardize temperature. We know the range of our measurement will not be sub zero temperatures so freezing temperature of water is a good reference point. Placing the thermocouple in an iced bath will calibrate it at 0°C. Since water boils at 100°C, we can use that as another reference point by placing the thermocouple inside a boiling pot of water. Our heater is rated to have maximum temperature of 760°C, therefore, our highest temperature is below that threshold. To found out the higher range, we heat up the disk plate without flow or rotation and surface temperature was found to be under 350°C by the used of infrared thermometer. Since there are no known material that has a melting point of around 350°C, and we do not have 10 thousand dollar for high temperature calibration machine. I will be using a heat gun a piece of copper and the infrared thermometer to do my calibration. I heat up the copper by the use of hot convective air from the heat gun until it is steady

state. For this condition, steady state means when I measured the surface temperature of copper at t=0 and at t=10 minutes, the temperature are within ±1°C. I was able to calibrate this number to be 537°C.

4.5 Validations

Measurement were validated with a computational model. Meng *et al.* created a computational model to simulate the effect of flow characteristics and heat transfer. [10] Meng created a model using the same specification as the experimental value. Taking consideration of energy losses in the system due to conduction, convection and radiate heat loss, we were able to have a very similar trend. The temperature were taken at an arbitrary distance above the surface and we choose to be 0.8mm. First comparison was when there the operating condition has no flow, and no rotation. The results are very similar as shown in Fig. 4.1. The second comparison what when the operating condition for both set to be 50.8mm inlet diameter with a rotational speed of 60 RPM and inlet flow velocity of 1 m/s. Again the result between the computational and experimental model is very similar as shown in Fig. 4.2.

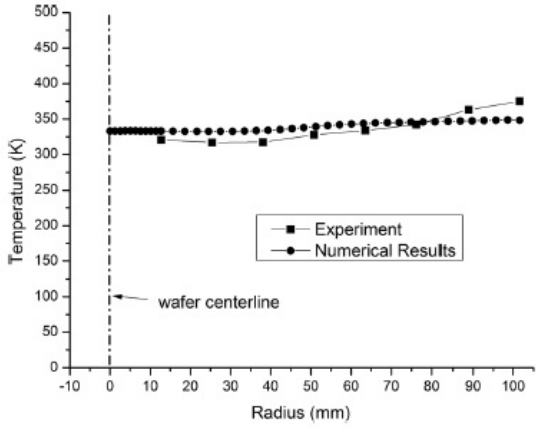

Figure 4.1: Computational and Experimental Comparison

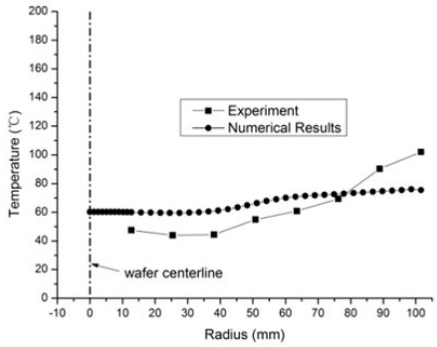

Figure 4.2: Computational and Experimental Comparison

Chapter 5

Results and Analysis

5.1 Introduction

This chapter will discuss about the results and analyze what the results means. As mentioned before, temperatures and velocities measurement were taken at various places in the reactor. Eight thermocouples were position above the heat disk plate for flow temperature near the substrate area. Five thermocouples were embedded inside the disk plate for recording heater temperature on the plate. Infrared thermometer were used to record surface temperatures since the unshielded thermocouples has problem reading when touching another metal. Rotameter was used to record flow rate and the inlet velocities. Hot wires anemometer was use to record the exit velocities and temperatures. Tachometer was used to record and maintain rotational speed. With all these measurement device recording all the data, it is important to break it down and convert the raw data into usable data that can be easier understand.

There are many parameters that will affect the temperature distribution across the disk. Parameters such as inlet diameter, inlet velocity and rotation speed are being study in this experiments. In the previous chapter, we mentioned about dimensionless numbers and what they mean. This chapter, we will use the raw data and express them in dimensionless forms for easier understanding of what is happening in the reactor. We will also show how changing a physical parameter changes the behavior of the flow characteristics and the heat transfer of the system. Effect of inlet diameter, effect of inlet velocity, and effect of rotation changes how the gas flows from inlet to outlet, it changes the recirculation effects, and it also changes the boundary layer near the surface. A control experiment was done to see the temperature above the plate.

Fig. 5.1 shows the temperature reading at various height above the heated plate.

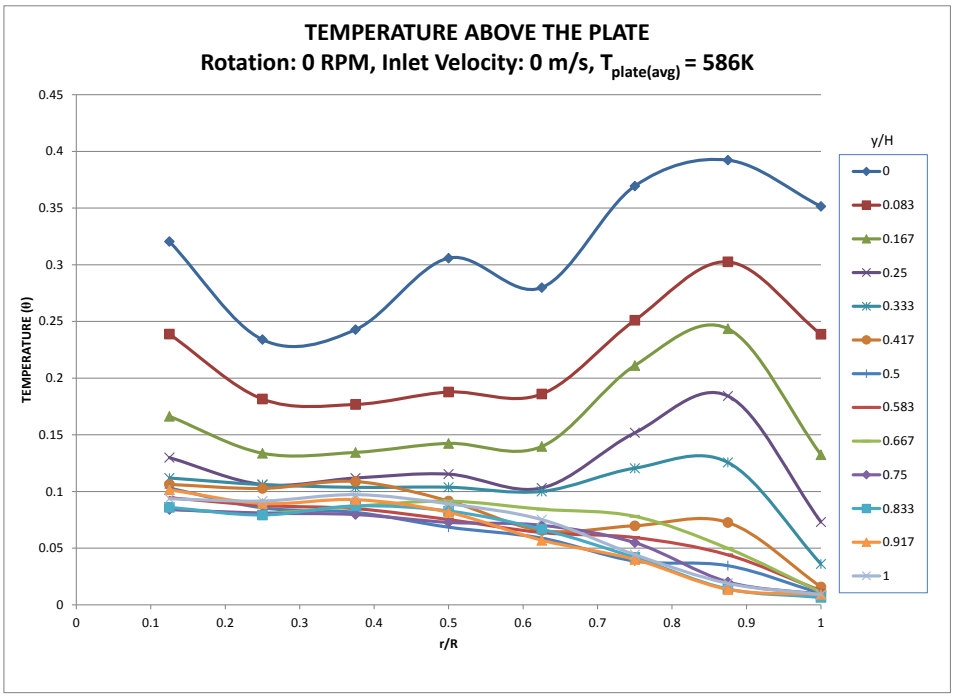

Figure 5.1: Flow Temperature, Rotation: 0RPM, Inlet Velocity: 0m/s

Average temperature of the plate is measured to be 586K. Since there is no flow, the fluctuation is the buoyancy driven flow within the system. Hot air rises from the center and recirculation of the hot air is shown when r/R value closer to 1. As the thermocouple moves away from the plate, temperature decreases to a very low value. Most of the lines collapse when y/H value is greater than 0.333. This indicates that the thermal boundary layer is about one third or 8.5mm thick from the total distance measured of 25.4mm. It is a good idea to measure in a small increment near the plate and increase the increment as it moves further away.

Another control experiment was a measuring temperature with respect to voltage. The reason we do this control experiment was to know the performance of the heater at steady state. Each measure was record after the temperature was in steady state. we waited 5 minute between each measure to ensure that it is steady state and by steady

state mean the fluctuation of temperature is ±2°. Each measurement was an average of multiple measurement that was recorded by the DAQ system.

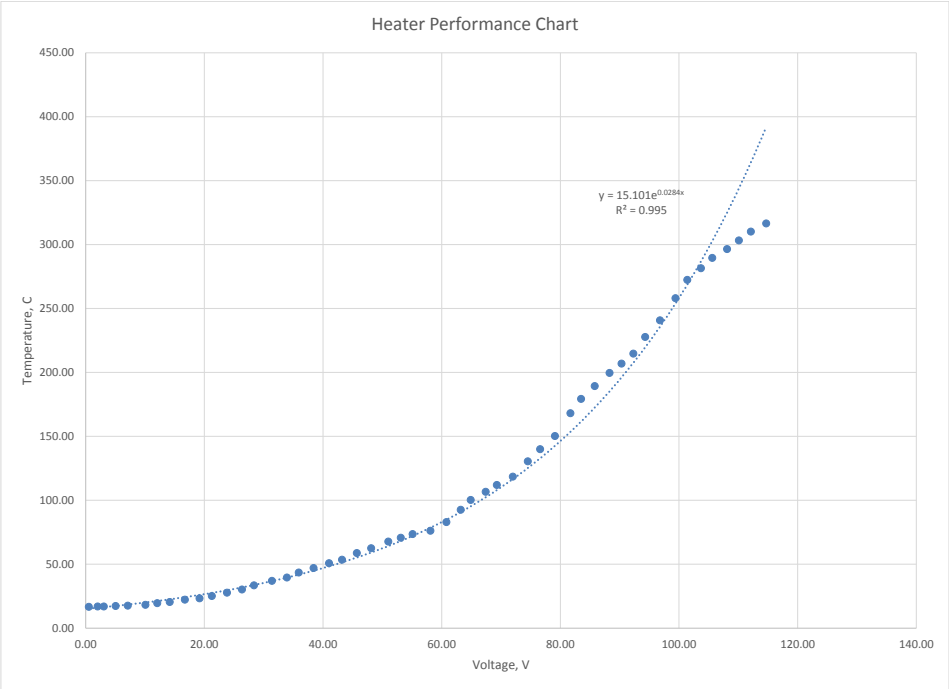

Figure 5.2: Heater Performance - Temperature at Various Voltage Inputs

After plotting the measured value, an exponential curve fit was use on the graph. R square value of 0.995 means that the heater increases temperature exponentially with voltage. An equation of the curve fit was also determined to be

$$T = 15.101e^{0.0284v} \tag{5.1}$$

Where, v is the voltage, and T is the output temperature.

There is one last control experiment that was done before we move on to changing parameters. This is the response time of the system. The response time is when the system reaches 90% of the full steady state temperature. The importance of response

time is to measure the speed of the system. This is the time it takes before the system becomes steady states again. For this test, we are incorporating rotational effect of 60RPM with 1 m/s inlet velocity and 25.4mm inlet diameter. The results of the system response time is found out to be around 5 minutes and 3 seconds. Therefore it will take around 5 minutes to get to 90% of the full scale. This number matches with the time it take until each measure is considered to be steady state on the previous control experiment. Now that the location of the boundary layer, system response time, and heater performance is known, we can now start looking at the effects when parameters are changed.

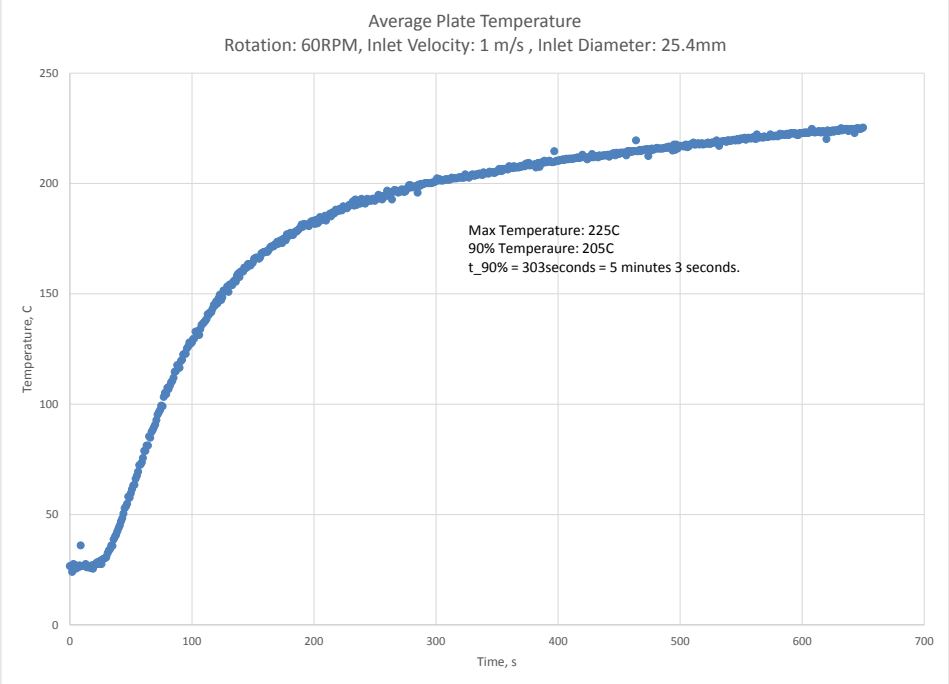

Figure 5.3: Response Time of the System

5.2 Effect of Inlet Diameter and Inlet Velocity

The first parameter we are varying is the inlet diameter. Inlet diameter effects the temperature distribution and the flow characteristic at the beginning of the system. We will be using a 25.4mm inlet and a 50.8mm inlet diameter. To show the effect of changing the inlet diameter, we hold the other parameter constants.

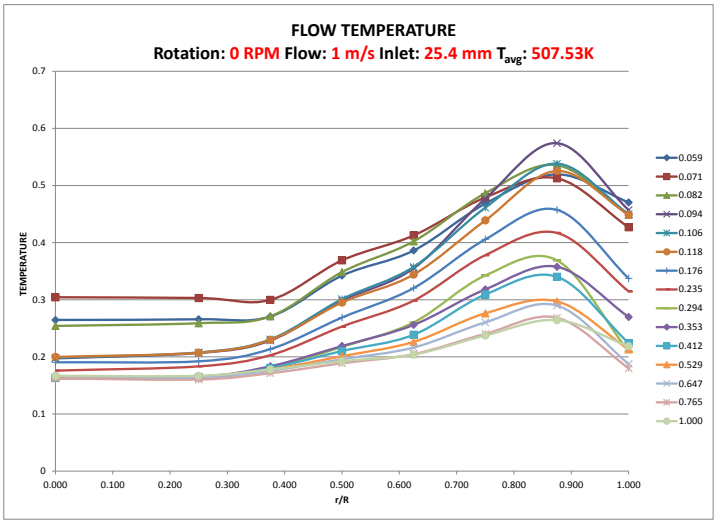

Figure 5.4: Flow Temperature- Rotation: 0 RPM, Inlet Velocity: 1 m/s, Inlet Diameter: 25.4mm

Looking at Fig. 5.4 and Fig. 5.5, we can see the recirculation effect is reduce. The lines are parallel indicating the reduction of recirculation. When the flow recirculates the temperature fluctuates since cooler air sinks and hotter air rises. Also the center temperature has been reduced because of the inlet diameter. Looking at Fig. 5.4, the temperature from 0.1 to 0.4 y/h is somewhat constant until greater than 0.4. It increases at a very rapid rate. However, if you look at Fig. 5.5, the increase is more subtle and it increases after the 0.4 y/h. Now we will look the change of the inlet diameter when we increased the flow velocity to 2 m/s.

In this two figures, the flow temperature behaves around the same as the previous two. Fig. 5.6 shows recirculation when it is near r/R = 1. Fig. 5.7 shows the smooth

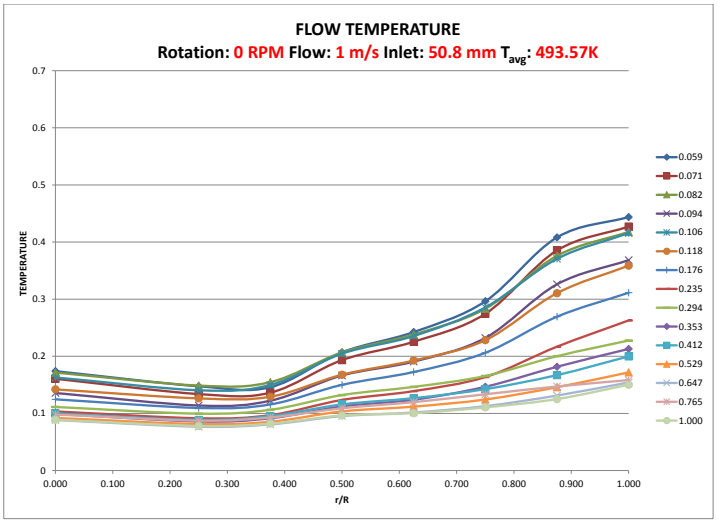

Figure 5.5: Flow Temperature- Rotation: 0 RPM, Inlet Velocity: 1 m/s, Inlet Diameter: 50.8mm

parallel lines and also noticed the overall exit temperature has been decreased. Smaller inlet diameter has a maximum exit temperature of 0.52 and the larger inlet dimater has an exit temperature of 0.35. This indication that the overall temperature of the system is decreased. This is due to the higher velocity and bigger inlet diameter. To keep the constant velocity, flow rate need to be increased. Fig. 5.8 below shows the flow rate for each of the case.

	25.4 mm	50.8mm
1 m/s	0.00051 m3/s	0.00202 m3/s
2 m/s	0.00101 m3/s	0.00405 m3/s

Figure 5.8: Volumetric flow rate requirement to maintain specific inlet velocity

Inlet velocity also effect the flow characteristics inside the reactor, similar to changing the inlet diameter. As we see in Fig. 5.8, flow rates increases as we increase velocity,

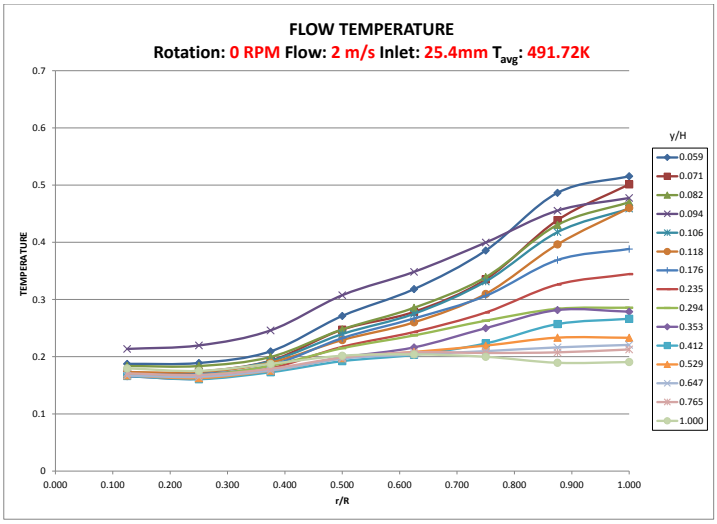

Figure 5.6: Flow Temperature- Rotation: 0 RPM, Inlet Velocity: 2 m/s, Inlet Diameter: 25.4mm

as well as flow rate increase as the diameter increase. Based on that figure, doubling the velocity only increase the flow rate by 200%, however doubling the diameter increases the flow rate by 400%. Now that we have flow rate, we can determine the Reynolds number of the flow. The Reynolds number is given as:

$$Re_{inlet} = \frac{4Q_{inlet}}{\nu \pi D_{inlet}} \tag{5.2}$$

The value is calculated using the respective flow rate and average temperatures to determine the kinematic viscosity. The Reynolds number for each case is tabulated below.

Observing Fig. 5.9,the Reynolds number for the 1 m/s case is laminar, but when the area or the inlet velocity increases the flow start to become turbulent. Reynolds number for inlet diameter of 25.4mm with inlet velocity of 2 m/s is the same as inlet diameter of 50.8mm with inlet velocity of 1 m/s even though the flow rates are different. Even though the flow rate are different, they are dynamically similar and they are both transitioning into the turbulent regime. Carefully looking at Fig. 5.5 and Fig. 5.6, you

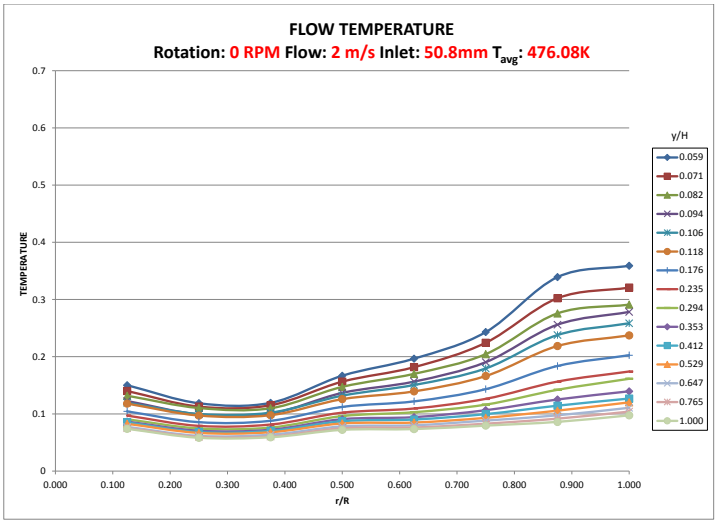

Figure 5.7: Flow Temperature- Rotation: 0 RPM, Inlet Velocity: 2 m/s, Inlet Diameter: 50.8mm

	25.4mm	50.8mm
1 m/s	1619.874049	3239.748098
2 m/s	3239.748098	6479.656042

Figure 5.9: Reynolds Number for the Corresponding Flow Rate

can see the average temperature of the two is approximately the same. The flow might not be identical but it has the same trend. For the case when inlet diameter is 50.8mm and inlet velocity is 2 m/s, the flow is fully turbulent.

Lastly we will look at the Richardson number of these 4 cases. Richardson number shows the effect of buoyancy in the reactor. Natural convection plays a strong role in this system. It induces a natural force that moves the flow. This phenomena is called buoyancy driven flow. As this buoyancy force increases in this system, the thermal boundary layer increases and the flow from the inlet might not penetrate close enough to the plate. This creates a barrier over the plate, and the thicker is the thermal

boundary layer the more chance the flow will separates and transition into turbulent flow. As the flow becomes turbulent, recirculation occurs and causes random flow patterns. Buoyancy is one of the causes to low deposition rate and uniformity problem in the CVD reactor. The Richardson number is defined as

$$Ri = \frac{Gr}{Re^2} \tag{5.3}$$

For this four case, Richardson number was calculated and it is shown in Fig. 5.10.

	25.4mm	50.8mm
1 m/s	11.46674746	2.738055075
2 m/s	2.689507999	0.614713272

Figure 5.10: Richardson Number for the Corresponding Flow Rate

Observing the table for Richardson number indicated that buoyancy dominates in all of the four cases shown earlier. This implies operating at those conditions will not yield a satisfactory results. We can conclude that for now that the larger the inlet diameter the better the results will be. Hence the reason why most modern CVD systems tries to incorporate as large of a inlet diameter as possible without losing the control of flow rates into the reactor chamber. Figures below shows few recent designs of CVD reactors.

5.3 Effect of Rotation

Rotation designs contribute a big role in the improvement of the CVD reactors. Taken from online sources, Fig. 5.11 [12] and Fig. 5.12 [13] both show rotational susceptor design integrated into their modern commerical reactor. The effect is based from basic fluid dynamics. When fluid flow over a stationary disk, the velocity near the surface will be zero. This is due to the viscos property of the fluid at the surface, and it is also called the no-slip condition. If the disk was rotating, the air near the surface would

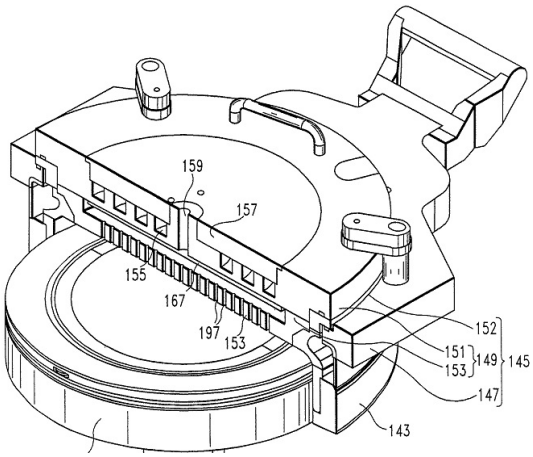

Figure 5.11: Applied Materials CVD Reactors. Adapted from Google Patent

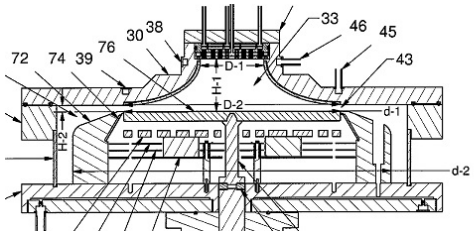

Figure 5.12: Valence Process Equipement CVD Reactors. Adapted from Google Patent

rotate the same speed as the disk. This induces a force into the flow, causing the rest of the flow in the region to rotate as well. The induced of centripetal force helps delay the flow separations inside the reactor chamber and also help to push the flow from the center to the edge and out of the reactor.

Comparing Fig. 5.5 when rotation at 0 RPM with Fig. 5.13 when rotation is at 60 RPM, it seems like there were no much changes in the system. The average temperature of the two is the same, maximum temperature closes to the plate are very similar in trend. However, if looking closely at measurement at other heights, it shows less intersecting lines on the 60RPM case. This is an indication that the flow is becoming more uniform. Lets increase the rotation to 120RPM and evaluate the results.

Observing Fig. 5.14, again there are not much change in the flow, however the overall temperature has decreased. Maximum temperature was close to the order of 0.5 for the 60 RPM case, but it is now around 0.45. There is also a distinctive separation in the temperature field. Between the height of y/H = 0.118 and y/H of 0.176, there is a big temperature drop across the entire length of the disk. This indicate that the thermal boundary layer is around the order of y/H = 0.118 or about 2.3 mm in thickness. Free stream area occurs at around y/H = 0.176 or about 3.35mm above the plate. Let increase the rotation to 300RPM and evaluate the results.

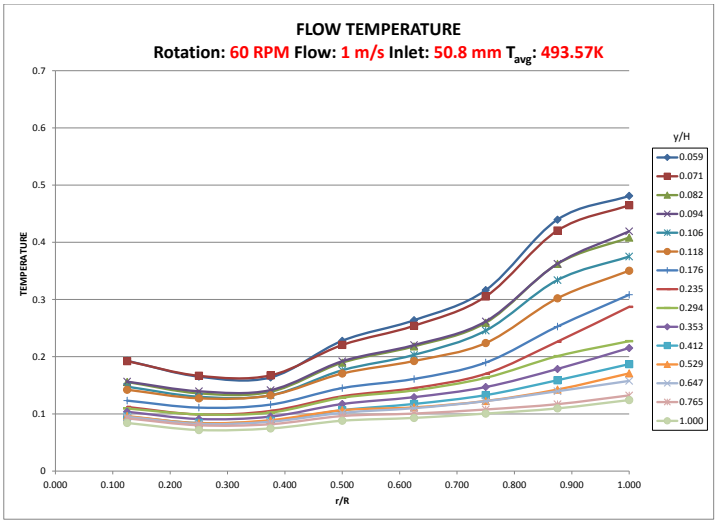

Figure 5.13: Flow Temperature- Rotation: 60 RPM, Inlet Velocity: 1 m/s, Inlet Diameter: 50.8mm

In Fig. 5.15, the average temperature continue to decrease indicating that it is losing thermal energy with the reactor. The maximum flow temperature also decreased. Highest measure at 0.38 compare to previous at 0.45. The flow uniformity also improved compared to the previous cases. The temperature gap between the y/H value of 0.118 and 0.176 also appears on this case. However, there is also another distinctive temperature gap from 0.176 and 0.235 that cannot be ignored. We can assume that the boundary layer is not larger than y/H = 0.235 or 4.5mm. Dandy *et al.* has done simulation to determine the boundary thickness in a CVD reactor. Even though operating condition are not identical, his results were found that at 1000K, the thermal boundary layer would be around 35mm.[4] However the trend is similar, so as the temperature decrease the thermal boundary layer also decrease for his simulations. His minimum temperature is 1000K, if we interpolate his data to 500K, it would decreased the thermal boundary layer even more. Now lets check the effect of inlet velocity again with rotation. Increasing inlet velocity along with a rotation will aid the flow even more.

Fig. 5.16 shows that increasing the velocity to 2 m/s with rotation changes the

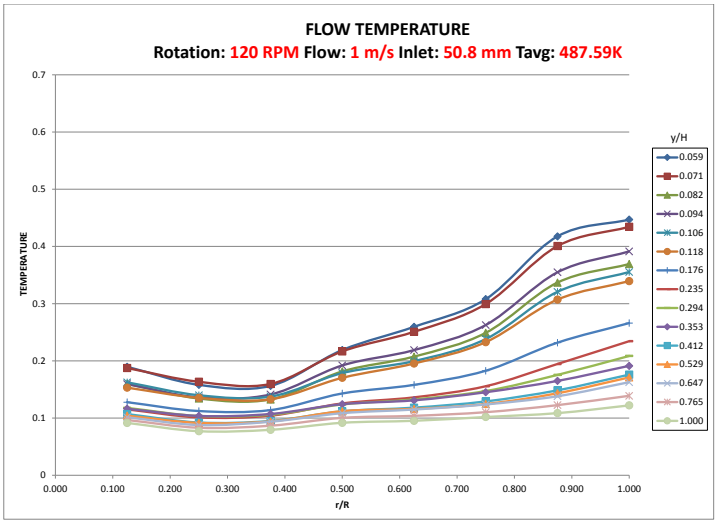

Figure 5.14: Flow Temperature- Rotation: 120 RPM, Inlet Velocity: 1 m/s, Inlet Diameter: 50.8mm

system even more. Average temperature decreased further to 454K from 493K when the flow velocity was at 1 m/s. Overall thermal energy decrease because the maximum flow temperatures is now around 0.3. The flow uniformity is better compared to the 1 m/s case. Closer examine the graph, shows that recirculation still occurs around y/H of 0.235 and 0.294 near the r/R 0.5 range. Lets increase the rotation speed to 300 RPM and evaluate the results.

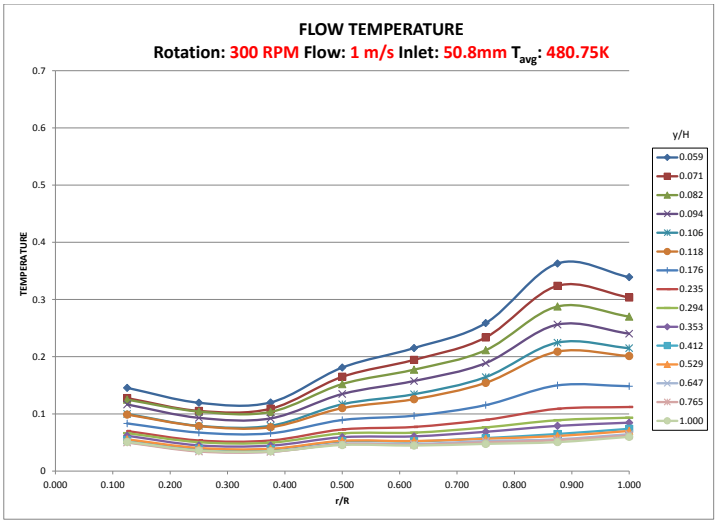

Figure 5.15: Flow Temperature- Rotation: 300 RPM, Inlet Velocity: 1 m/s, Inlet Diameter: 50.8mm

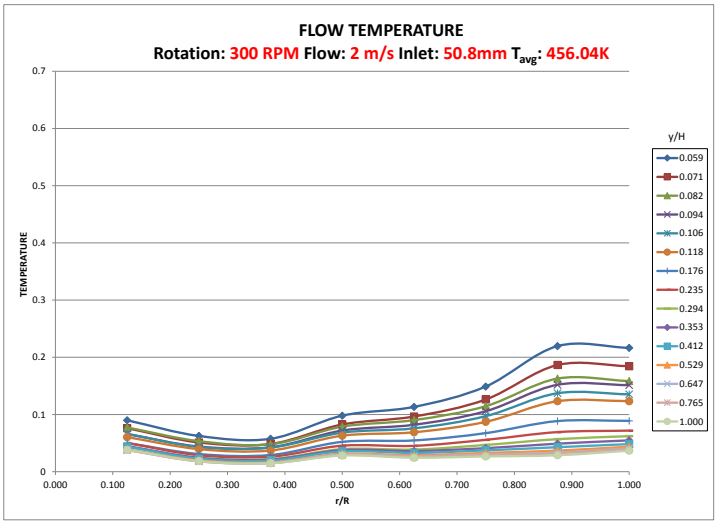

Figure 5.17: Flow Temperature- Rotation: 300 RPM, Inlet Velocity: 2 m/s, Inlet Diameter: 50.8mm

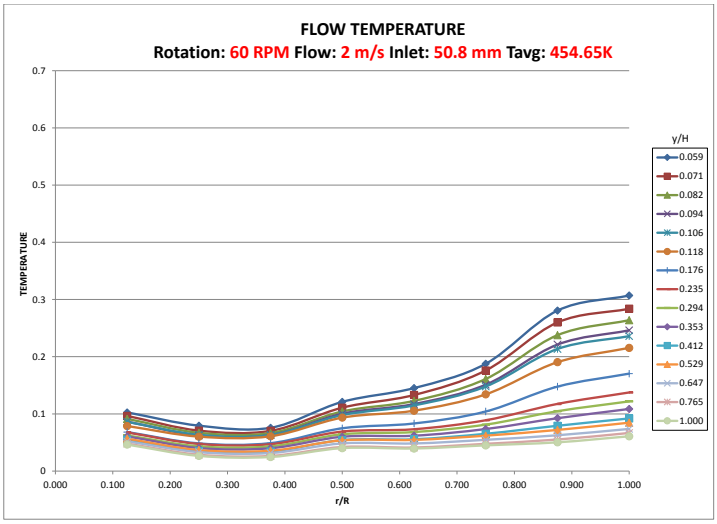

Figure 5.16: Flow Temperature- Rotation: 60 RPM, Inlet Velocity: 2 m/s, Inlet Diameter: 50.8mm

Fig. 5.16 continue to show improvements to the flow characteristics. The Temperature profile are not crossing and it is very uniform. The uniformity of the temperature profile indicate that buoyancy force may no longer play a role in this condition. Average temperature did not decrease compared to the 60 RPM case. However overall temperature inside the reactor has decreased, indicating a decrease in thermal energy. To further examine the boundary layer, we will look at the exit velocity distribution between 60RPM and 300RPM. Measurement were taken at various height at exit.

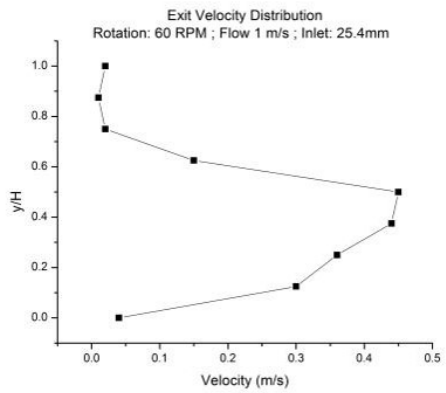

Figure 5.18: Exit Velocity Distribution at Exit - Rotation 60RPM

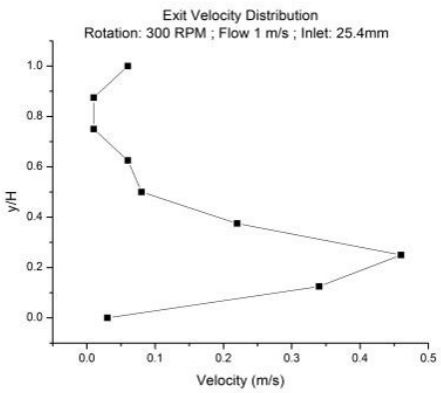

Figure 5.19: Exit Velocity Distribution at Exit - Rotation 300RPM

Fig. 5.18 shows the steep drop in velocity at around y/H value of 0.65, and at the same time when y/H is close to 0, the velocity is almost 0. The sharp increase and decrease of velocity between the region y/H 0 and 0.65 indicate that the boundary layer is present. For Fig. 5.19, when the rotation speed is a 300RPM, the sharp increase and decrease of velocity is also present. However, the range of this fluctuation is between the y/H value of 0 and 4.5, indicating a smaller boundary layer thickness. This shows higher rotation speed help reduces buoyancy effect. To further demonstrate the importance of rotation in a CVD reactor, we calculated the Richardson number across every case and see the comparison.

Rotation Per Minute (RPM)	**Inlet Diameter:** 25.4 mm **Flow Speed :** 1 m/s	**Inlet Diameter:** 25.4 mm **Flow Speed :** 2 m/s	**Inlet Diameter:** 50.8 mm **Flow Speed :** 1 m/s	**Inlet Diameter:** 50.8 mm **Flow Speed :** 2 m/s
0	11.46674746	2.689507999	2.738055075	0.614713272
60	2.718871997	1.275414499	1.298436421	0.583031217
120	1.359435998	0.637707249	0.649218211	0.291515608
300	0.543774399	0.2550829	0.259687284	0.116606243

Figure 5.20: Richardson Number Comparison For All Cases

When Richardson number is greater than 10, buoyancy effect dominates and when Richardson number is less than 0.1, buoyancy effect is negligible. In Fig. **??** shows that at no rotation, slow inlet velocity, and small inlet diameter buoyancy dominates. When the rotational speed is at 300 RPM and at the higher inlet velocity and higher inlet diameter setting, the value is close to 0.1 indicating that buoyancy effect becomes negligible. Further examine the temperature field by looking a flow visualizations and temperature gradient to prove the importance of rotational effect in a CVD reactor.

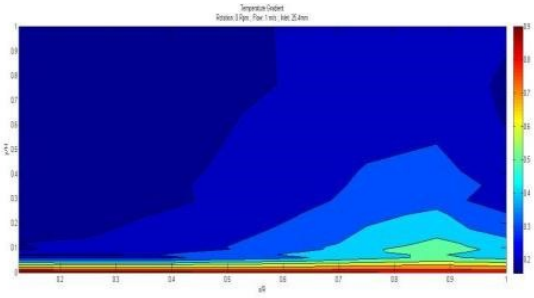

Figure 5.21: Temperature Gradient - 60RPM

Figure 5.22: Flow Visualization - 60RPM

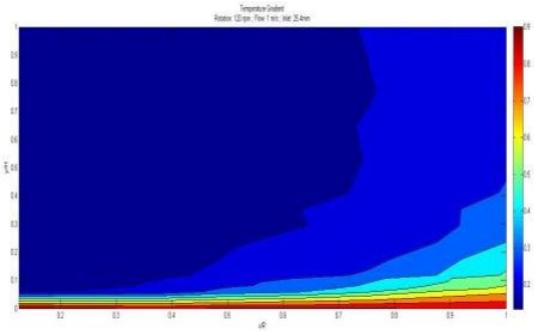

Figure 5.23: Temperature Gradient - 300RPM

Figure 5.24: Flow Visualization - 300RPM

Looking at the visual of the smoke in Fig. 5.3, you can see the smoke rising from the plate and recirculating. The thickness of the smoke also looks very thick. However, looking at Fig. 5.3, the smoke is very uniform and only near the surface and no recirculation. The smoke on the surface is swirling because of the higher speed rotational effect.

Chapter 6

Conclusions

In this thesis, a detailed experiment was setup to study and investigate the flow characteristics and heat transfer in a rotating chemical vapor deposition reactor. CVD is a heat activated process that allow material to break down atomically and recombine to form layers of crystalline structures. Maintaining the proper flow rate of the gases, temperature of the heater and the pressure of the system is very important to the quality of the film growth. Therefore, it is important to understand the importance of these operating parameters and how it affect the outcome. A simple rotating CVD reactor was built for this study. Motors and motor controllers was used in controlling the motion of all the equipment. Flow and temperature measuring sensors was coupled with a DAQ system and it was integrated into the reactor for monitoring and data acquisitions.

Measuring the temperatures, flow rates, and flow velocities can determine the flow characteristic and heat transfer in the reactor. Using these collected data, we can interpret if the flow is laminar or turbulent, as well as if buoyancy force dominate or force convection dominates inside the reactor. We can also determine the effect when changing operating parameters such as inlet velocity, inlet diameters, and different rotational speed. Reactors without rotational susceptor experience a harder time controlling the flow across the substrate, because of the buoyancy force generated from the heated disk. Even with a higher inlet velocity and larger inlet diameter, the buoyancy effect dominates the force convection. This buoyancy force creates the randomness in a CVD reactor. It will cause uniformity problems, and it will also cause deposition problems as the recirculation gas might be outside of the growth regime.

As we started to increase the rotational parameter, the flow evens out and become

less random. The rotational induces a force into the flow that aids the buoyancy effect. It pushes the flow from the center out across the disk and out of the system. Combine this with the higher velocity and large inlet diameter, buoyancy effect became negligible. Richardson number was found to be greater than 11 when reactor was no rotating, and the same Richardson number decreases to the order of 0.1 when the operating condition was 300 RPM with the higher inlet velocity and larger inlet diameter. Even though we know that increasing those operating condition improves the flow characteristics and heat transfer, we know that at one point the improvement will stop and start to effect the flow and heat transfer in a negative way.

One example is when inlet diameter is too large, it is harder to control the flow rate into the reactor. Another example is when inlet velocity is too large also implies that the mass flow rate is large as well. Material wont have enough time for the chemical reaction to take place, and it would be wasting material. Even when the rotational speed is too high, the centrifugal force created will cause uniformity problem as well since the rotational effect pushes the flow outward from the center. There is an optimal operating condition for every experiment. Validating an experimental results with a computational result will help reduce the cost when optimizing the operating conditions since the only resource waste is computing time rather than the high expensive raw materials. Therefore, for the future work, we will be looking into the quality of the material at different operating conditions. We want to optimize these growth condition by use of computational models as well as improving experimental model from computational results.

Bibliography

[1] J.F. Foss C. Tropea, A.L. Yarin. *Springer Handbook of Experimental Fluid Mechanics*. Springer, New York, NY, 2007.

[2] Richards Cristy Jaluria Yogesh Chiu, Wilson. Experimental and numerical study of conjugate heat transfer in a horizontal channel heated from below. *Journal of Heat Transfer*, 123:688–697, 2001.

[3] J. R. Creighton and P. Ho. Introduction to chemical vapor deposition. *Chemical Vapor Deposition*, 2001.

[4] David S. Dandy and Jungheum Yun. Momentum and thermal boundary-layer thickness in a stagnation flow chemical vapor deposition reactor. *Journal of Materials Research*, 12:1112–1121, 1997.

[5] N. Ernest Dorsey and Churchill Eisenhart. On absolute measurement. *The Scientific Monthly*, LXXVII:49–55, 1953.

[6] J. G. Eden. *Film Deposition by Plasma Techniques*. J. L. Vossen and W. Kern, Academic Press, New York, 1991.

[7] Churchill Eisenhart. Realistic evaluation of the precision and accuracy of instrument calibration systems. *JOURNAL OF RESEARCH of the National Bureau of Standards*, 670.

[8] M. Konuma. *Thin Film Processes II*. Springer-Verlag, New York, 1992.

[9] Nasir Memon. Flow structure and heat transfer in an impinging jet cvd reactor. Master's thesis, Rutgers University, Graduate School- New Brunswick, 2009.

[10] Wong S Jaluria Y Meng, J. Fabrication of gallium nirtide films in a chemical vapor deposition reactor. *Journal of Thermal Science and Engineering Applications*, 7.

[11] Fujio Terai, Hiroaki Kobayashi, Shuji Katsui, Naoki Tamaoki, Takao Nagatomo, and Tetsuya Homma. High-speed rotating-disk chemical vapor deposition process for in-situ arsenic-doped polycrystalline silicon films. *Japanese Journal of Applied Physics*, 44(11R):7883, 2005.

[12] Google USPTO. 300mm cvd chamber design for metal-organic thin flim deposition, 1999.

[13] Google USPTO. Chemical vapor deposition reactor, 2014.

[14] Wenliang Wang, Weijia Yang, Zuolian Liu, Yunhao Lin, Shizhong Zhou, Huirong Qian, Fangliang Gao, and Guoqiang Li. Epitaxial growth of high quality aln films on metallic aluminum substrates. *CrystEngComm*, 16:4100–4107, 2014.

[15] T. C. Xenidou, A. G. Boudouvis, N. C. Markatos, D. Samlor, Franois Senocq, N. Prud'Homme, and Constantin Vahlas. An experimental and computational analysis of a mocvd process for the growth of al films using dmeaa. *Surface and Coatings Technology*, 201:8868–8872, 2007.

[16] Anthony H. McDaniel Jill Troup Yongkee Chae, William G. Houf and Mark D. Allendorf. Stagnation flow reactor investigation of tin oxide cvd from monobutyltin trichloride. *Journal of The Electrochemical Society*, 151:527–534, 2004.